Available online at www.sciencedirect.com
ScienceDirect
Journal of the European Ceramic Society 30 (2010) 2617–2624
www.elsevier.com/locate/jeurceramsoc

Structure and physical properties of nickel manganite $NiMn_2O_4$ obtained from nickel permanganate precursor

Alejandra Díez [a], Rainer Schmidt [b], Aurora E. Sagua [a], Marisa A. Frechero [c], Emilio Matesanz [d], Carlos Leon [b], Emilio Morán [e,*]

[a] Departamento de Química, Laboratorio de Fisicoquímica Inorgánica, Universidad Nacional del Sur, 8000 Bahía Blanca, Argentina
[b] Departamento de Fisica Aplicada III, GFMC, Universidad Complutense, 28040 Madrid, Spain
[c] Departamento de Química, CONICET-Fisicoquímica, Universidad Nacional del Sur, 8000 Bahía Blanca, Argentina
[d] Centro de Difracción de Rayos X, Universidad Complutense, 28040 Madrid, Spain
[e] Departamento de Química Inorgánica, Facultad de Ciencias Químicas, Universidad Complutense, 28040 Madrid, Spain

Received 11 December 2009; received in revised form 9 April 2010; accepted 23 April 2010
Available online 31 May 2010

Abstract

In this paper we present the structural, magnetic and dielectric properties of ceramic nickel manganite $NiMn_2O_{4+\delta}$ produced by using nickel permanganate $Ni(MnO_4)_2xH_2O$ as a precursor. We have characterized the $NiMn_2O_{4+\delta}$ stoichiometry using quantitative energy-dispersive analysis of X-rays and thermal gravimetry under reducing conditions. Increased oxygen and Mn^{4+} contents were detected. X-ray diffraction and Rietveld refinement of X-ray data were carried out. Temperature dependent magnetization measurements were performed and the ferri-magnetic transition was identified at ≈100 K. The ferri-magnetic moment was found to be $\approx 1\mu_B$ and hysteretic magnetization vs applied field curves were obtained. Dielectric properties were measured using impedance spectroscopy. Two dielectric relaxation processes were detected, which were associated with grain boundary and bulk contributions. The Arrhenius plots of resistivity and the temperature dependent dielectric permittivity were obtained for the two relaxations by means of an equivalent circuit model based on a series of two parallel RC elements.

Keywords: B. X-ray methods; C. Chemical properties; C. Magnetic properties; C. Dielectric properties. E. Thermistors

1. Introduction

Complex manganese oxides have recently evoked strong interest in various structures with different Mn valence states and Mn coordinations for example in perovskites, spinels, or pyrochlores. The manganites display a vast range of fascinating electrical and magnetic properties (colossal magnetoresistance, ferromagnetism, charge ordering and many more), which often come about due to the mixed valence states of manganese. Nickel manganite $NiMn_2O_4$ exhibits a partially inverse cubic spinel structure, which is well known since many years.[1–3] $NiMn_2O_4$ is widely used in industry as the basis for the production of ceramic temperature sensors due to its electrical properties characterized by a negative temperature coefficient (NTC) of the semi-conducting electrical resistance.[4–10] Several dopants can be included to improve the sensor performance.[11–13] Despite the apparent spinel structure and simple chemical formula this material is surprisingly complex and keeps nowadays being revisited and prepared by different routes and in different forms: powder, thin and thick films, and single crystals.[14–21] The complexity of this compound is partially owned to the variability of the Ni and Mn lattice positions. Ni and Mn cations can both occupy tetrahedral and octahedral crystal sites, which are both interstitial sites within the cubic closed packed oxygen sub-lattice of the spinel structure.

The fraction of Ni occupancy on the octahedral sites corresponds to the inversion parameter v of the cubic spinel structure, which has a strong effect on the Mn valence states: The Ni fraction moving to octahedral sites is compensated by Mn going to tetrahedral sites. Such tetrahedral Mn has valence state 2+, because Mn^{3+} is unfavourable in tetrahedral four-fold coordina-

* Corresponding author.
E-mail addresses: rainerxschmidt@googlemail.com (R. Schmidt), emoran@quim.ucm.es (E. Morán).

0955-2219/$ – see front matter © 2010 Elsevier Ltd. All rights reserved.
doi:10.1016/j.jeurceramsoc.2010.04.032

tion. The formation of tetrahedral Mn^{2+} is compensated by an equal amount of Mn^{4+} on the octahedral sites in order to retain charge balance, thus leading to an internal disproportionation. The driving forces for this disproportionation process are (1) the preferred octahedral coordination of Ni^{2+}, and (2) the preferential 4+ valence state of Mn (t_{2g}^3) in an octahedral coordination: an increasing amount of octahedral Mn^{3+} ($t_{2g}^3 e_g^1$) would lead to energetically unfavourable Jahn–Teller lattice distortions and ultimately to tetragonal symmetry of the spinel.

It has been found previously that v is in fact dependent on the synthesis or sintering temperature. Both, v and the Mn valence therefore depend on the preparation route and thermal history, and the physical properties vary accordingly. Thus, a common objective in many previous publications was to correlate details of the synthesis route, structure and microstructure with the observed charge transport and magnetic properties.[5,6,22–27] The use of $Ni(MnO_4)_2xH_2O$ as a precursor is interesting due the high Mn^{7+} oxidation state. In conventional ceramic processing routes, precursor oxides such as Mn_2O_3 are used where the initial Mn valence is 3+, which corresponds to the expected average Mn valence in $NiMn_2O_4$. We show in this work that the permanganate precursor allows fabricating $NiMn_2O_4$ materials with typical physical properties.

In a previous paper we have shown that principally nickel permanganate can be used as a precursor for the synthesis of $NiMn_2O_4$.[28] $Ni(MnO_4)_2xH_2O$ was shown to be thermally unstable, which is typical for permanganates. The compound is particularly suitable for use as a precursor for $NiMn_2O_4$ production, because it provides the fixed 1:2 cationic Ni:Mn ratio required. The permanganates are well known to be highly oxidizing: for $Ni(MnO_4)_2xH_2O$ it was found that E° Mn (VII)/Mn (IV) = 1.69 V.

As concerns a possible non-stoichiometry of $NiMn_2O_{4+\delta}$, the literature is abundant. A stoichiometric compound has often been reported ($\delta = 0$), as well as non-stoichiometric variations: mostly cationic vacancies ($Ni_xMn_{3-x}\square_{3\delta/4}O_{4+\delta}$)[29-33] have been mentioned, where δ depends on x and the synthesis conditions. Reports on oxygen vacancies also exist.[31,34] Therefore, we have made considerable effort in this study to correctly represent the stoichiometry and crystal structure of $NiMn_2O_{4+\delta}$ produced via the permanganate route. Furthermore, we have comprehensively determined the physical properties by means of temperature dependent magnetization and dielectric property measurements.

2. Experimental

The crystallization and the thermal decomposition of the $Ni(MnO_4)_2{\cdot}6H_2O$ precursor have been described previously in Ref. 28. Here, we have followed this coprecipitation method where aqueous solutions of barium permanganate and nickel sulphate were mixed together and $BaSO_4$ precipitated out and was separated by filtration. The remaining solution was evaporated at 55–60 °C and the resulting nickel permangante precursor ground and calcined in air at 900 °C for 24 h resulting in $NiMn_2O_{4+\delta}$, which was slow cooled to ambient conditions by turning off the furnace.

X-ray pattern of synthesized $NiMn_2O_{4+\delta}$ powder were collected on a Panalytical B.V. X'pert PRO ALPHA 1 instrument with fast X'Celerator detector operating at 45 kV and 40 mA, fitted with a primary curved Ge 111 monochromator in order to get Cu Kα1 radiation (λ = 1.5406 Å). For cell parameter measurements and phase identification, the angle step and counting time were 0.033° (2θ) and 9 s, respectively. For Rietveld refinement analysis, XRD pattern were taken over long periods (28 h) and fitted using Fullprof software.[35] Sample morphology and grain sizes were examined by means of scanning electron microscopy (SEM) performed on a Jeol 6400 microscope equipped with a detector for energy-dispersive analysis of X-rays (EDAX) for quantitative characterization.

The oxygen stoichiometry was determined by thermogravimetric analysis up to 600 °C using a Cahn balance in a H_2/He atmosphere (100 Torr H_2, P_{total} = 0.5 bar), whereby the intermediate and final residues had been characterized by XRD phase analysis.

Magnetic measurements were performed in a SQUID-Quantum Design magnetometer. Susceptibility was measured as a function of temperature between 4 and 300 K at a fixed magnetic field of 1000 Oe. The sample was zero field cooled (ZFC) and magnetization measured during heating. Furthermore, magnetization was measured as a function of applied field (up to 5 T) well below the Curie temperature at 25 K.

Impedance spectroscopy (IS) was carried out on 900 °C sintered pellets, which were covered on both sides with Au electrodes using dc sputtering. IS was performed at 150–320 K between 10 Hz and 2 MHz. An Agilent E4980A LCR meter and an Oxford Instruments closed-cycle He refrigerator were used. The data was obtained in terms of the real and imaginary parts of the complex impedance (Z'–Z'').

A $NiMn_2O_{4+\delta}$ control sample was produced via the conventional precursor oxide route: NiO (Alfa Aesar 99+%) and Mn_2O_3 (Fisher 99%) were thoroughly ground and synthesized at 1100 °C for 12 h in air. The resulting powders were ground, pressed into pellets and sintered at 1100 °C in air. After sintering at 1100 °C the temperature was reduced and held at 850 °C for 60 h in order to restore phase purity. It has been shown previously that such an annealing process can re-incorporate NiO into the spinel structure, which segregates out at high temperatures such as 1100 °C.[1] After annealing the pellet was quench-cooled to room temperature.

3. Results and discussion

3.1. Morphology and oxygen stoichiometry

The $NiMn_2O_{4+\delta}$ powder produced from the permanganate precursor route consists of distinct ceramic grains as can be seen in the SEM micrograph in Fig. 1. The grain sizes are of the order of 1 μm and the samples were found to be homogeneous. Chemical analysis was performed by EDAX using the K-lines of the respective elements on a well crystallized powder. The cation ratio of Ni: Mn was found to be 1:1.99 in excellent agreement with the expected 1:2 proportion. The oxygen content from EDAX was found to be unreliable.

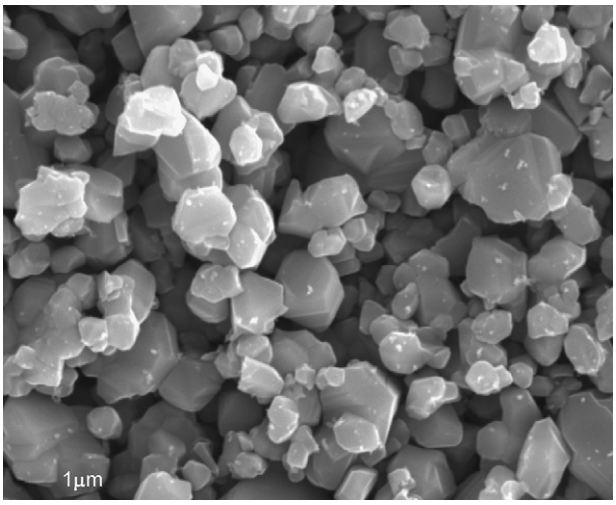

Fig. 1. Scanning electron micrograph of representative nickel manganite powder obtained by the thermal decomposition of hexahydrated nickel permanganate.

However, the oxygen stoichiometry in $NiMn_2O_{4+\delta}$ is an important parameter, because it determines the average oxidation state of manganese, if it is assumed that Ni has a valence of 2+ and reduced or oxidized Ni^{1+}/Ni^{3+} may be unlikely to occur. Thermal gravimetry of $NiMn_2O_{4+\delta}$ was carried out in reducing atmosphere: 0.5 bar of He/H_2. Decomposition takes place in two steps (Fig. 2) and the final residues were Ni and MnO as confirmed by XRD phase analysis. The first step at ≈325 °C corresponds to the formation of a rock-salt phase of formula $Ni_{1-S}Mn_SO$ according to the XRD pattern, whereas the second step at ≈500–600 °C (1b) represents the reduction of the rock-salt phase to nickel metal and MnO. The reduction process may be expressed as:

$$NiMn_2O_{4+\delta} + (1+\delta)H_2 \rightarrow 3Ni_{1/3}Mn_{2/3}O + (1+\delta)H_2O \uparrow \quad (1a)$$

$$3Ni_{1/3}Mn_{2/3}O + H_2 \rightarrow Ni + 2MnO + H_2O \uparrow \quad (1b)$$

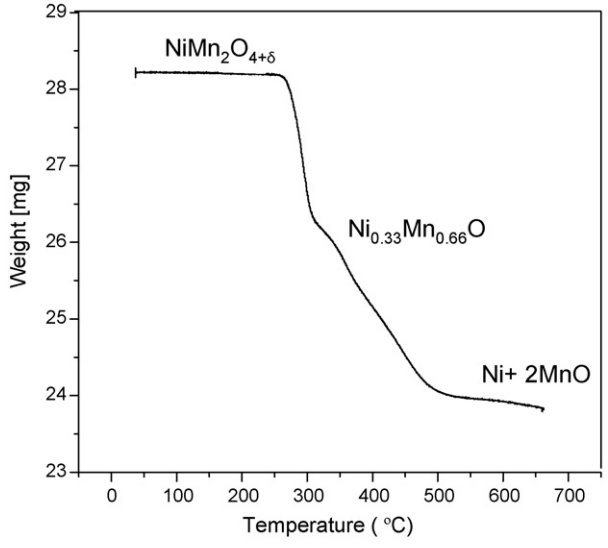

Fig. 2. Thermogravimetric analysis performed on representative nickel manganite powder under He/H_2.

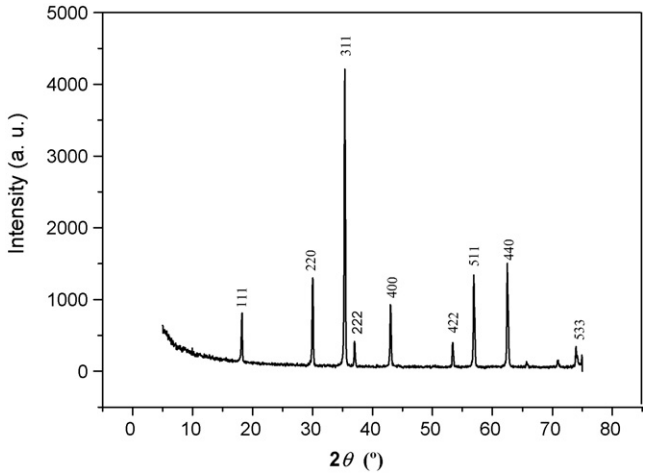

Fig. 3. Powder X-ray diffraction pattern of $NiMn_2O_{4+\delta}$ produced from nickel permanganate precursor fired at 900 °C in air. Miller indexes correspond to a cubic spinel of parameter $a = 8.380$ Å.

From the weight of the final products the δ value was determined to be 0.20(5) indicating oxygen excess. The only plausible mechanism to compensate for such oxygen excess is by cationic vacancies, whereas the second possibility of intersticial oxygen may be highly unlikely for steric reasons: oxygen anions are closed packed in a spinel structure. The existence of such cation vacancies has been confirmed previously in the literature,[29–33] whereas intersticial oxygen has never been observed in an oxide spinel to the best of our knowledge. This δ value of 0.20 corresponds to an average Mn oxidation state of 3.2 and is a strong indication for increased Mn^{4+} content, assuming an oxidation state of 2+ for Ni. The presence of Mn^{3+} on tetrahedral sites as a result of $Mn^{2+} \rightarrow Mn^{3+}$ oxidation is unlikely as mentioned above. The apparent extra oxygen and increased average Mn valence may be a result of the slow cooling process across the instability region of $NiMn_2O_{4+\delta}$ at $T \approx 450$–750 °C, where oxidation occurs.[1] An additional explanation may be the high Mn^{7+} valence state in the precursor.

3.2. X-ray diffraction and Rietveld refinements

XRD pattern of the permanganate precursor were in agreement with the literature[28]: $Ni(MnO_4)_2 \cdot 6H_2O$. After calcination at 900 °C in air, the XRD patterns of the $NiMn_2O_{4+\delta}$ product (Fig. 3) correspond to the cubic spinel phase with a lattice parameter a close to 8.38 Å, in good agreement with values reported in the literature ($a = 8.3790$ Å, ICDD-pdf card 88-0241 and $a = 8.40$ Å, ICDD-pdf card 71-0852).[36,37] We have performed Rietveld refinement analysis of an XRD pattern from a well crystallized powder. Analysis was performed in the cubic *Fd*-3*m* space group and starting values for the atom positions and unit cell size were obtained from previous work on single crystal $NiMn_2O_4$ (ICDD-pdf card 84517).[14] Fig. 4A shows the experimental and refined patterns and their differences. Cell parameters, agreement factors, refined atomic coordinates and calculated main interatomic distances and angles are sum-

Table 1
Results obtained from the Rietveld analysis.

Crystal data		
Phases	$NiMn_2O_4$	NiO
Crystal system	Cubic	Cubic
Space group	*FD*-3*M*	*Fm*-3*m*
a (Å)	8.38138(3)	4.17738(5)
V (Å^3)	588.770(3)	72.897(1)
R_B	1.75	10.4
R_F	1.63	7.22
Fract (%)	97.1(4)	2.90(6)

Parameter	Refinement
R_P	3.75
W_P	5.12
R_{exp}	4.60
χ^2	1.24

Atomic positional parameters and thermal displacement amplitudes together with site occupation factors for $NiMn_2O_4$

Site	Ion	*x*	*y*	*z*	Biso	SOF	*W* position
O1	O^{2-}	0.2621(1)	0.2621(1)	0.2621(1)	1.73(5)	0.167	32e
Mn1	Mn^{2+}	0.125	0.125	0.125	0.37(3)	0.036	8a
Ni1	Ni^{2+}	0.125	0.125	0.125	0.37(3)	0.004	8a
Mn2	Mn^{3+}	0.5	0.5	0.5	0.50(2)	0.011	16d
Mn3	Mn^{4+}	0.5	0.5	0.5	0.50(2)	0.036	16d
Ni2	Ni^{2+}	0.5	0.5	0.5	0.50(2)	0.036	16d

$NiMn_2O_4$ distances and angles

(Mnl, Nil)–O (Å)	1.9872(1)
(Mn2, Mn3, Ni2)–O (Å)	2.0007(2)
O–(Mnl, Nil)–O (°)	109.47(9)
O–(Mn2, Mn3, Ni2)–O (°)	180.0(1)

marized in Table 1. An excellent fit was obtained only by including NiO as a second phase, in agreement with previous work.[38,39] In our case the content of NiO is 2.90% and may be interpreted as the predicted segregation of NiO out of the spinel $NiMn_2O_{4+\delta}$ structure at 900 °C.[1] In the literature 950 °C is usually quoted for the onset temperature of NiO segregation. Our results suggest that such segregation already takes place at 900 °C to a small extent. The NiO second phase was reflected in the refinement by Ni deficiency on the tetrahedral sites. Refinement of a fully stoichiometric structure within the solid solution of $Ni_{1-x}Mn_{2+x}O_4$ gave clearly higher fitting errors. Therefore, we favour a small amount of Ni vacancies on the tetrahedral sites. Such Ni vacancies would be compensated most likely by oxygen vacancies, because the second possible mechanism, Mn oxidation, is unlikely at high temperatures of ≈900 °C, which are usually associated with a reducing ambient. However, such oxygen vacancies would most likely disappear during the slow cooling process across the oxidizing region at $T \approx 450$–750 °C. A possible excess of oxygen, as detected by thermal gravimetry, and the possible presence of additional Ni or Mn cation vacancies could not be refined unambiguously from X-ray data due to the insensitivity of the method to the oxygen positions. Fig. 4B shows evidence for the small extra NiO phase on the XRD pattern profile: the diffraction peaks at approximately 37.2° and 43.2° show a double peak structure, where the high angle "pump" can be associated with NiO.

No indications for other secondary phases were found, despite the slow cooling process of our samples across the oxidizing region of 450–750 °C. A relatively large inversion parameter *v* of 0.865 was found, which is typical for slow cooled samples.[2]

To summarize the results obtained by the Rietveld analysis, the formula of this inverse spinel can be expressed as:

$$(Ni^{2+}_{0.0965}Mn^{2+}_{0.865})_{Th}[Ni^{2+}_{0.865}Mn^{3+}_{0.265}Mn^{4+}_{0.865}]_{Oh}O_4 \quad (2)$$

where () indicate tetrahedral (Th) and [] octahedral (Oh) sites. As mentioned before, the apparent oxygen excess was neglected in this representation.

3.3. Magnetization measurements

ZFC magnetic susceptibility vs temperature measurements with an applied field of 1 kOe indicated a ferri-magnetic transition at about $T_C \approx 100$ K (Fig. 5A). Plotting the inverse susceptibility as a function of temperature in the paramagnetic region, approximately linear Curie-Weiss behaviour was found (Fig. 5B). The observed Curie constant is 4.92 emu K/mol and the experimental magnetic moment is 6.27 Bohr magnetons (μ_B). Both, T_C and the magnetic moment are smaller

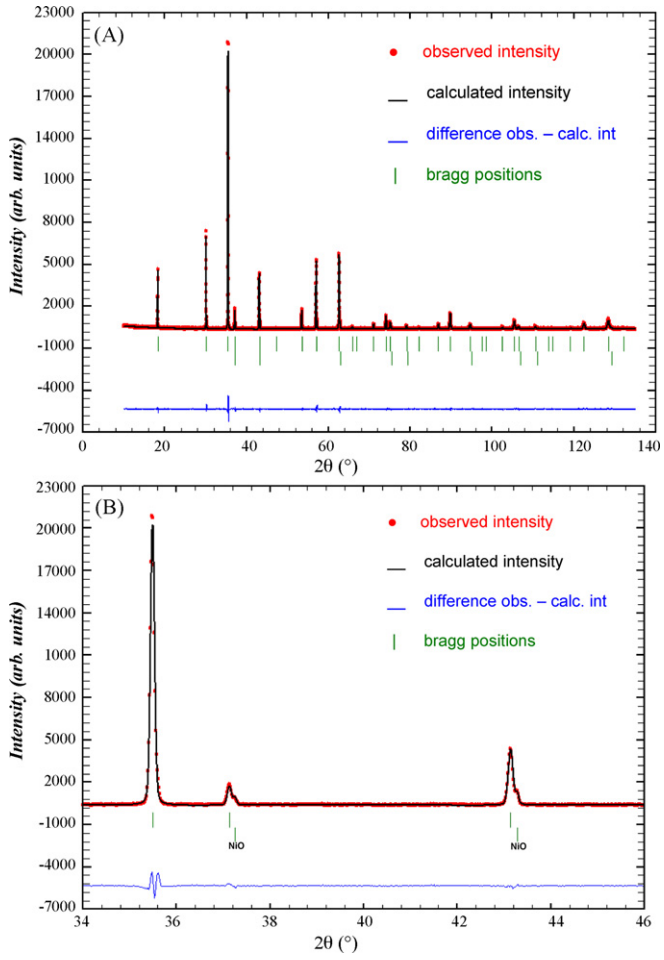

Fig. 4. (A) Rietveld fitting on powder X-ray diffraction data. Calculated and experimental intensities and their differences are shown. (B) Details on the data demonstrating the presence of secondary phase NiO due to a double peak structure of $NiMn_2O_{4+\delta}$ (2 2 2) and (4 0 0) reflections. NiO reflections are indicated, all other reflections correspond to $NiMn_2O_{4+\delta}$.

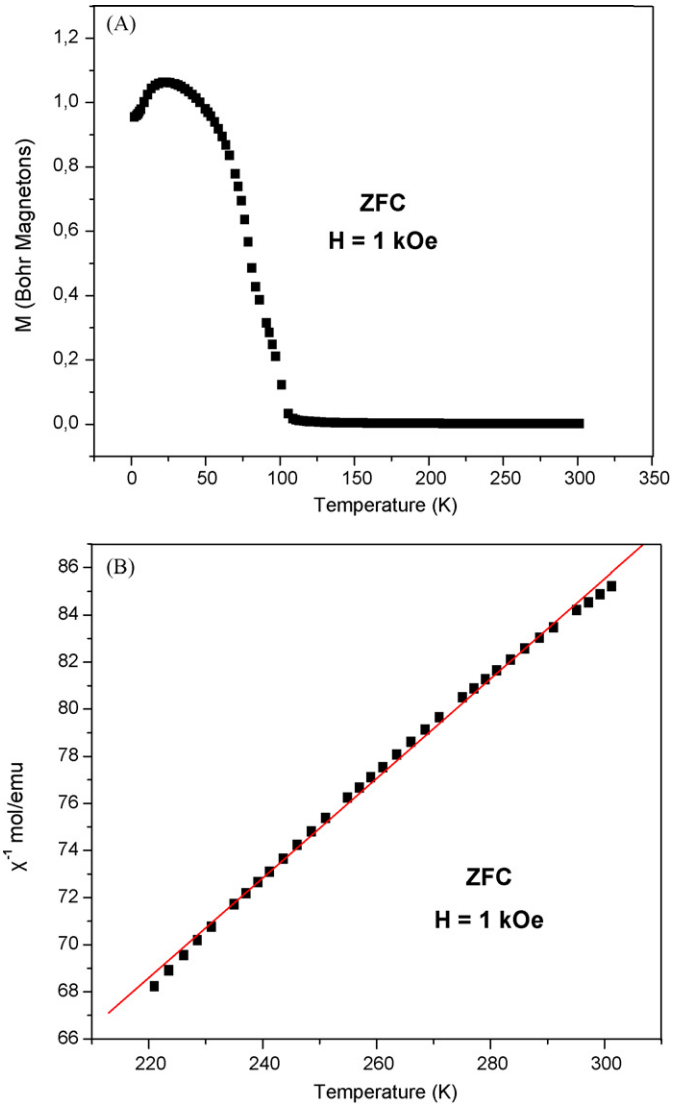

Fig. 5. (A) Magnetic susceptibility vs temperature plot at constant field of 1000 Oe. (B) ZFC inverse susceptibility vs temperature in the paramagnetic region.

than previously reported,[14,40,41] which may be associated with increased Mn^{4+} ($3\mu_B$) content and the concomitant decrease in Mn^{3+} ($4\mu_B$) content. This is in agreement with the oxygen over-stoichiometry and resulting cationic vacancies suggested above (Section 3.1). The negative value of the Weiss temperature $\theta = -118$ K points to predominantly anti-ferromagnetic interactions.

The ferri-magnetic interactions were investigated by magnetization measurements as a function of the applied field at constant temperature of 25 K well below T_C (Fig. 6A). A characteristic weak ferri-magnetic hysteresis loop was found and a saturation magnetization of $M_s \approx 1\mu_B$ could be estimated. Magnetization does not saturate at high fields and varies almost linearly with H, which points towards the presence of a paramagnetic contribution, possibly from NiO impurities. In fact, NiO was shown previously to be magnetic if nano-sized.[42] The coercive field is relatively low in the order of 150 Oe. The experimental M_s value is in reasonable agreement with an estimate from the Néel co-linear model: M_s was calculated by adding all contributions on the octahedral sites ($Ni^{2+} = 2\mu_B$; $Mn^{2+} = 5\mu_B$; $Mn^{3+} = 4\mu_B$; $Mn^{4+} = 3\mu_B$) and subtracting the corresponding contributions on the tetrahedral sites according to Eq. (2), which yields $0.87\mu_B$. The measured M_s value of $\approx 1\mu_B$ is slightly larger than the theoretical value possibly due to contributions from impurities.

3.4. Impedance spectroscopy

Complex impedance spectroscopy data was obtained in terms of real (Z') and imaginary (Z'') parts of the impedance. In Fig. 7 the complex impedance plot of $-Z''$ vs Z' displays two slightly overlapping semi-circles, which can be associated with two relaxation processes. The relaxations were assigned to an intrinsic bulk and a grain boundary (GB) contribution. An equivalent circuit was used (shown in Fig. 7) in order to fit the data at various temperatures yielding the bulk resistance (R1) and capacitance (CPE1), and the GB resistance (R2) and capacitance (CPE2). Conventionally, an ideal relaxation process is modelled with an ideal RC element of parallel resistance and capacitance,[43] and

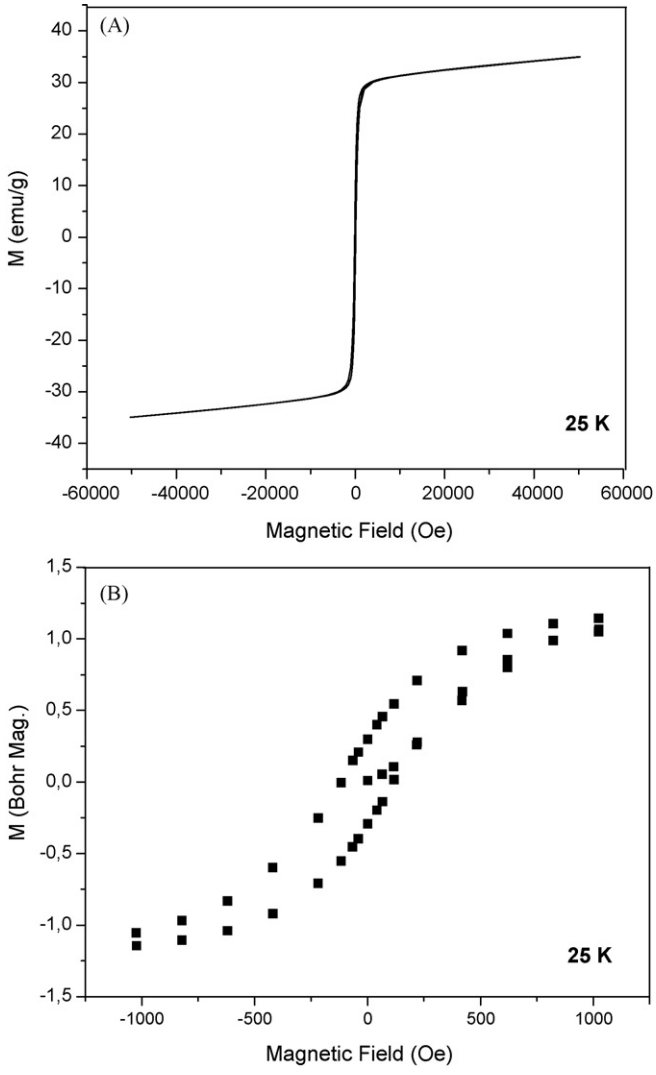

Fig. 6. (A) Magnetization vs applied magnetic field at 25 K. (B) High resolution curve of magnetization vs applied field at 25 K.

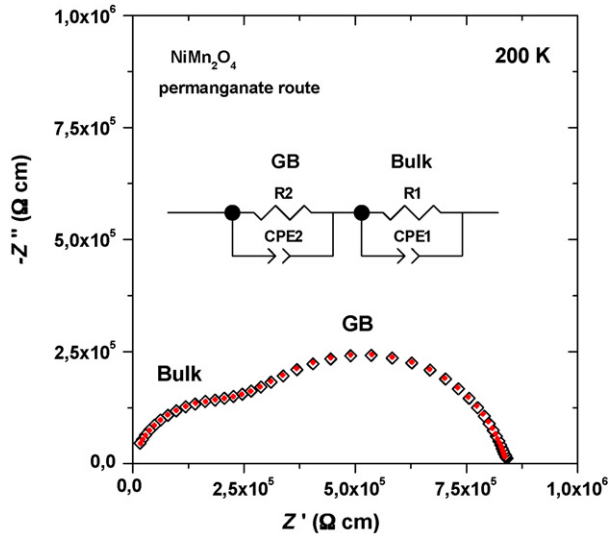

Fig. 7. Complex plane plot of $-Z''$ vs Z' at 200 K and equivalent circuit model. Data (◊) and model (♦) show excellent agreement.

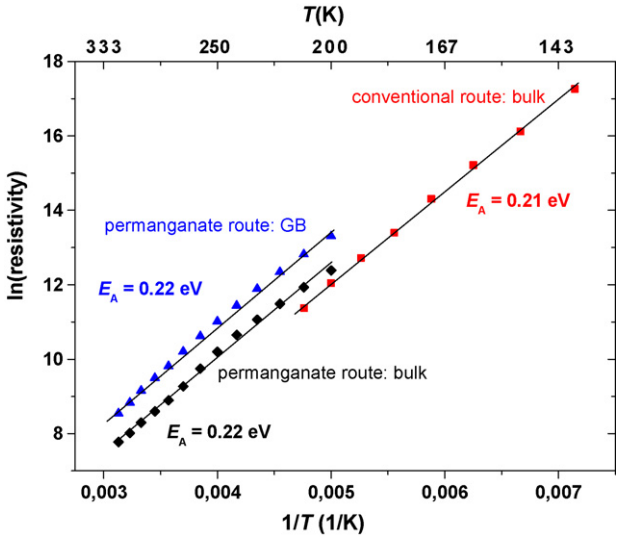

Fig. 8. Arrhenius plots of bulk (♦) and GB (▲) resistivity obtained from equivalent circuit fits; for comparison the bulk resistivity of a conventionally synthesized sample is shown (■).

for GB and bulk relaxations two RC elements can be simply added in series. We have encountered non-ideal behaviour here, which manifests itself by slightly suppressed semi-circles.[44] This can be accounted for by replacing the ideal capacitor with a constant phase element (CPE).[45] In our case, an almost ideal fit was obtained and the data and model show excellent agreement (Fig. 7). The CPE capacitance values were corrected to conventional capacitance given in [F/cm].[46] The bulk and GB resistance values obtained from the temperature dependent fits were normalized to the pellet geometry and were plotted on Arrhenius axes shown in Fig. 8. Additionally, the bulk resistivity from the conventional and quench-cooled $NiMn_2O_{4+\delta}$ pellet is shown. The activation energies were determined as the gradients of the various Arrhenius plots. It can be seen that GB and bulk activation energies are similar in $NiMn_2O_{4+\delta}$ from permanganates, and further, both are similar to the bulk activation energy from conventional $NiMn_2O_{4+\delta}$. It appears that the charge transport mechanism is qualitatively unchanged for GB and bulk areas, and for samples from different production routes. However, clear quantitative changes can be seen where the permanganate sample has a clearly higher bulk resistivity as compared to the conventional sample. We associate this with a higher Mn^{4+} content, and the Mn^{3+}/Mn^{4+} ratio may be further away from the ideal 1:1 ratio, which is the most favourable to support Mn^{3+}/Mn^{4+} localized electron hopping. Such localized Mn^{3+}/Mn^{4+} small polaron hopping has been suggested previously to be the basis of charge transport in $NiMn_2O_{4+\delta}$.[5,47] Mn^{2+} cations on tetrahedral sites are expected to not participate to the hopping process, because donation of an electron would lead to an oxidation state of Mn^{3+}, which is very unlikely to occur in tetrahedral 4 coordinate environments. The relative dielectric permittivity ε_r is shown in Fig. 9. The intrinsic bulk ε_r is in the range of 30–50, whereas the GB permittivity is in the range of 300. Both values are rather typical for such type of relaxations.[43] The bulk permittivity in the slow-cooled perman-

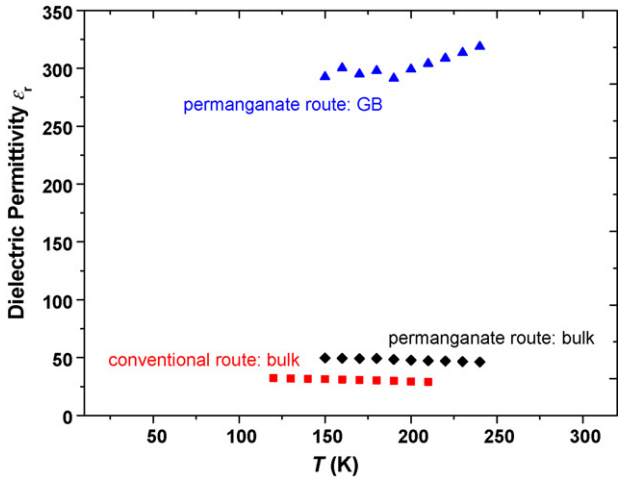

Fig. 9. Bulk (♦) and GB (▲) relative dielectric permittivity from equivalent circuit fits; for comparison the bulk permittivity (■) of a conventional sample is shown.

ganate sample is slightly higher as compared to conventional and quench-cooled production routes. As mentioned before, the increased Mn^{4+} content may be compensated by cation vacancies, which may have lead to more flexibility in the lattice for ionic displacements as a response to the applied voltage signal, thus leading to higher intrinsic bulk permittivity.

4. Concluding remarks

In conclusion, we have shown that the choice of a permanganate precursor oxide for the synthesis of $NiMn_2O_{4+\delta}$ is appropriate and leads to typical magnetic and dielectric properties. The $NiMn_2O_{4+\delta}$ investigated showed increased oxygen and Mn^{4+} content, which led to a reduction in the anti-ferromagnetic moment and T_C, and an increase in intrinsic bulk resistivity and bulk dielectric permittivity.

Acknowledgment

This work was supported by grants from the Comisión de Investigaciones Científicas de la Provincia de Buenos Aires (CIC), Consejo Nacional de Investigaciones Científicas y Técnicas (CONICET) and Universidad Nacional del Sur (UNS) in Argentina and projects (MAT 2004-03070-CO5-05, MAT 2007-31034) granted by the Ministerio de Ciencia e Innovación (MINCINN) in Spain. R.S. wishes to acknowledge the Ministerio de Ciencia e Innovacion in Spain for granting a Ramon y Cajal Fellowship. The authors wish to express their gratitude to Dr. Julio Romero de Paz (Universidad Complutense Madrid) for technical assistance with the magnetic measurements, to Prof. Alario-Franco (UCM) for carefully reading this manuscript, Dr. Ian Terry (University of Durham) for useful discussions and Prof. Derek C. Sinclair for allowing use of impedance spectroscopy facilities.

References

1. Wickham DG. Solid-phase equilibria in the system NiO–Mn_2O_3–O_2. *J Inorg Nucl Chem* 1964;**26**:1369.
2. Boucher BP, Buhl R, Perrin M. Etude cristallographique du manganite spinelle cubique $NiMn_2O_4$ par diffraction de neutron. *Acta Cryst B* 1969;**25**:2326.
3. Boucher B, Buhl R, Perrin M. Structures Magnetiques et etude des proprietes Magnetiques des Spinelle cubiques $NiMn_2O_4$. *J Phys Chem Solids* 1970;**31**:363.
4. Martin De Vidales JL, Garcia-Chain P, Rojas RM, Vila E, Garcia-Martinez O. Preparation and characterization of spinel-type Mn–Ni–Co–O negative temperature coefficient ceramic thermistors. *J Mater Sci* 1998;**33**(6):1491–6.
5. Fritsch S, Sarrias J, Brieu M, Couderc JJ, Baudour JL, Snoeck E, Rousset A. Correlation between the structure, the microstructure and the electrical properties of nickel manganite negative temperature coefficient (NTC) thermistors. *Solid State Ionics* 1998;**109**:229.
6. Csete de Gyoergyfalva GDC, Nolte AN, Reaney IM. Correlation between microstructure and conductance in NTC thermistors produced from oxide powders. *J Eur Ceram Soc* 1999;**19**:857.
7. Schmidt R, Basu A, Brinkman AW, Klusek Z, Datta PK. Electron-hopping modes in $NiMn_2O_{4+\delta}$ materials. *Appl Phys Lett* 2005;**86**(7):073501.
8. Guillemet-Fritsch S, Salmi J, Sarrias J, Rousset A, Schuurman S, Lannoo A. Mechanical properties of nickel manganites-based ceramics used as negative temperature coefficient thermistors (NTC). *Mater Res Bull* 2004;**39**(12):1957–65.
9. Veres A, Noudem JG, Perez O, Fourrez S, Bailleul G. Manganese based spinel-like ceramics with NTC-type thermistor behaviour. *Solid State Ionics* 2007;**178**(5–6):423–8.
10. Feteira A. Negative temperature coefficient resistance (NTCR) ceramic thermistors: an industrial perspective. *J Am Ceram Soc* 2009;**92**(5):967–83.
11. Shpotyuk O, Kovalskiy A, Mrooz O, Shpotyuk L, Pechnyo V, Volkov S. Technological modification of spinel based $CuxNi_{1-x-y}Co_{2y}Mn_{2-y}O_4$ ceramics. *J Eur Ceram Soc* 2001;**21**:2067.
12. Veres A, Noudem JG, Perez O, Fourrez S, Bailleul G. The effect of manganese substitution to gallium on the physical properties of $MgGa_{2-x}Mn_xO_4$ spinel type ceramic thermistors. *J Eur Ceram Soc* 2007;**27**(13–15):3873–6.
13. Zhao C, Wang B, Yang P, Winnubst L, Chen C. Effects of Cu and Zn co-doping on the electrical properties of $Ni_{0.5}Mn_{2.5}O_4$ NTC ceramics. *J Eur Ceram Soc* 2008;**28**(1):35–40.
14. Asbrink S, Waskowska A, Drozd M, Talik E. Physical properties and X-ray diffraction of a $NiMn_2O_4$ single crystal below and above the ferrimagnetic transition at T_c = 145 K. *J Phys Chem Solids* 1997;**58**:725.
15. Schmidt R, Brinkman AW. Preparation and characterisation of $NiMn_2O_4$ films. *Int J Inorg Mater* 2001;**3**:1215.
16. Schmidt R, Stiegelschmitt A, Roosen A, Brinkman AW. Screen printing of coprecipitated $NiMn_2O_4$ for production of NTC thermistors. *J Eur Ceram Soc* 2003;**23**(10):1549–58.
17. Hou Y, Huang Z, Gao Y, Ge Y, Wu J, Chu J. Characterization of $Mn_{1.56}Co_{0.96}Ni_{0.48}O_4$ films for infrared detection. *Appl Phys Lett* 2008;**92**(20):202115.
18. Schmidt R, Basu A, Brinkman AW. Production of NTCR thermistor devices based on $NiMn_2O_{4+\delta}$. *J Eur Ceram Soc* 2004;**24**(6):1233–6.
19. Jagtap S, Rane S, Gosavi S, Amalnerkar D. Preparation, characterization and electrical properties of spinel-type environment friendly thick film NTC thermistors. *J Eur Ceram Soc* 2008;**28**(13):2501–7.
20. Hrovat M, Belavic D, Kita J, Holc J, Cilensek J, Drnovsek S. Thick-film NTC thermistors and LTCC materials: the dependence of the electrical and microstructural characteristics on the firing temperature. *J Eur Ceram Soc* 2009;**29**(15):3265–71.
21. Ryu J, Kim K-Y, Choi J-J, Hahn B-D, Yoon W-H, Lee B-K, Park D-S, Park C. Highly dense and nanograined $NiMn_2O_4$ negative temperature coefficient thermistor thick films fabricated by aerosol-deposition. *J Am Ceram Soc* 2009;**92**(12):3084.
22. Ponce J, Rios E, Rehspringer JL, Poillerat G, Chartier P, Gautier JL. Preparation of nickel aluminium-manganese spinel oxides $Ni_xAl_{1-x}Mn_2O_4$ for oxygen electrocatalysis in alkaline medium: comparison of properties stemming from different preparation methods. *J Solid State Chem* 1999;**145**:23.

23. Gillot B, Kharroubi M, Metz R, Legros R, Rousset A. Electrical properties and cationic distribution in cubic nickel manganite spinels $Ni_xMn_{3-x}O_4$, $0.57 < x < 1$. *Solid State Ionics* 1991;**44**:275.
24. Yokoyama T, Abe Y, Meguro T, Komeya K, Kondo K, Kaneko S, Sasamoto T. Preparation and electrical properties of sintered bodies composed of monophase spinel $Mn_{(2-X)}Co_{2X}Ni_{(1-X)}O_4$ $(0 < x < 1)$ derived from rock-salt-type oxides. *Jpn J Appl Phys* 1996;**35**:5775.
25. 25 Islam MS, Catlow CRA. Structural and electronic properties of $NiMn_2O_4$. *J Phys Chem Solids* 1988;**49**:119.
26. Macklen ED. Electrical conductivity and cation distribution in nickel manganite. *J Phys Chem Solids* 1986;**47**(11):1073.
27. Brabers VAM, Terhell JCJM. Electrical conductivity and cation valencies in nickel manganite. *Phys Status Solidi (A)* 1982;**69**:325.
28. Schmidt JA, Sagua AE, Bazán JC, Prat MR, Braganza ME, Morán E. Nickel permanganate as a precursor in the synthesis of a $NiMn_2O_4$ spinel. *Mater Res Bull* 2005;**40**(4):635–42.
29. Tang X-X, Manthiram A, Goodenough JB. $NiMn_2O_4$ revisited. *J Less-Common Met* 1989;**156**:357.
30. Feltz A, Töpfer J. Bildung von Defektspinellen und Phasenbeziehungen im System $Ni_xMn_{3-x}O_4$. *Z Anorg Allg Chem* 1989;**576**:71.
31. Lisboa-Filho PN, Bahout M, Barahona P, Moure C, Pena O. Oxygen stoichiometry effects in spinel-type $NiMn_2O_{4-d}$ samples. *J Phys Chem Solids* 2005;**66**(7):1206–12.
32. Laberty C, Marquez-Alvarez C, Drouet C, Alphonse P, Mirodatos C. CO oxidation over nonstoichiometric nickel manganite spinels. *J Catal* 2001;**198**:266.
33. Drouet C, Alphonse P, Rousset A. Synthesis and characterization of non-stoichiometric nickel-copper manganites. *Solid State Ionics* 1999; **123**:25.
34. Jung J, Töpfer J, Mürbe J, Feltz A. Microstructure and phase development in $NiMn_2O_4$ spinel ceramics during isothermal sintering. *J Eur Ceram Soc* 1990;**6**:351.
35. Rodriguez-Carvajal J. FULLPROF suite. In: *Satellite Meeting of the XVth Congress of the International Union of Cryst*. 1990.
36. Faber J, Fawcett T. The powder diffraction file: present and future. *Acta Cryst B* 2002;**58**:325.
37. Belsky A, Hellenbrandt M, Karen VL, Luksch P. New developments in the inorganic crystal structure database (ICSD): accessibility in support of materials research and design. *Acta Cryst B* 2002;**58**:364.
38. Csete de Györgyfalva GDC, Reaney IM. Decomposition of $NiMn_2O_4$ spinels. *J Mater Res* 2003;**18**:1301.
39. Ashcroft G, Terry I, Gover R. Study of the preparation conditions for $NiMn_2O_4$ grown from hydroxide precursors. *J Eur Ceram Soc* 2005;**26**:901.
40. Peña O, Moure C, Bodenez V, Cailleaux X, Piriou B, Ortiz J, Zuñiga G, Gautier JL, Lisboa-Filho PN. Magnetic properties of spinel-type oxides $NiMn_{2-x}Me_xO_4$. *J Chil Chem Soc* 2005;**50**(3):617.
41. Peña O, Ma Y, Barahona P, Bahout M, Durán P, Moure C, Baibich MN, Martinez G. Magnetic properties of $NiMn_{2-x}Co_xO_4$ spinel oxides. *J Eur Ceram Soc* 2005;**25**(12):3051–4.
42. Parada C, Moran E. Microwave-assisted synthesis and magnetic study of nanosized Ni/NiO materials. *Chem Mater* 2006;**18**(11):2719–25.
43. Irvine JTS, Sinclair DC, West AR. Electroceramics: characterization by impedance spectroscopy. *Adv Mater* 1990;**2**(3):132.
44. Ross Macdonald J. *Impedance spectroscopy*. New York: John Wiley & Sons; 1987.
45. Schmidt R, Brinkman AW. Studies of the temperature and frequency dependent impedance of an electroceramic functional oxide thermistor. *Adv Funct Mater* 2007;**17**(16):3170.
46. Hsu CH, Mansfeld F. Technical note: concerning the conversion of the constant phase element parameter Y_0 into a capacitance. *Corrosion* 2001;**57**(9):747.
47. Schmidt R, Basu A, Brinkman AW. Small polaron hopping in spinel manganates. *Phys Rev B* 2005;**72**(11):115101.